Construction and Building Materials 234 (2020) 117336

Contents lists available at ScienceDirect

Construction and Building Materials

journal homepage: www.elsevier.com/locate/conbuildmat

Carbonation of concrete with construction and demolition waste based recycled aggregates and cement with recycled content

I.F. Sáez del Bosque [a,*], P. Van den Heede [b], N. De Belie [b], M.I. Sánchez de Rojas [c], C. Medina [a,*]

[a] School of Engineering, University of Extremadura, UEX-CSIC Partnering Unit, Institute for Sustainable Regional Development (INTERRA), 10003 Cáceres, Spain
[b] Magnel Laboratory for Concrete Research, Ghent University, Technologiepark Zwijnaarde 904, B-9052 Ghent, Belgium
[c] Eduardo Torroja Institute for Construction Science, UEX-CSIC Partnering Unit, C/ Serrano Galvache, 28033 Madrid, Spain

HIGHLIGHTS

- The mean carbonation depth in recycled concretes is 1.07–1.20 times greater than conventional concretes.
- The CO_2 penetration coefficient is below the mm/year$^{0.5}$ "good quality concrete".
- The minimum design cover could be reduced in member manufactured with the new concretes.
- The inclusion of MRA and OPC-CW does not compromise reinforcement passivity.

ARTICLE INFO

Article history:
Received 7 June 2019
Received in revised form 15 October 2019
Accepted 18 October 2019
Available online 7 November 2019

Keywords:
Recycled aggregate
Supplementary cementitious materials
Carbonation
Service life
Concrete

ABSTRACT

Durability is a major concern in concrete (particularly recycled concrete) structures exposed to carbonation-induced corrosion, given the social, economic, environmental and safety implications involved. This article explores carbonation performance in concrete with 25% or 50% mixed recycled construction and demolition waste aggregate, alone or in conjunction with cement containing 25% fired clay construction and demolition waste. Irrespective of cement type, the mean carbonation depth was slightly greater in materials with 25% or 50% recycled aggregate than in concretes with 100% natural aggregate, although the difference was not statistically significant for the 25% replacement ratio. In all the concretes studied, the carbonation coefficient was below the 4 mm/yr$^{0.5}$ indicative of good quality. Based on the prediction model proposed in Spain's concrete code, reinforcement passivity was guaranteed in all these types of concrete when exposed to class XC1 to XC4 carbonation environments for substantially longer than their 100 year design service life.

1. Introduction

Structural durability in concrete is an issue of increasing relevance, for the legislation in place on the subject [1–4] mirrors social demands for satisfactory performance throughout the service life of buildings and civil works, to minimise repairs not envisaged in their maintenance plans [5,6]. Enhanced durability (in this case, higher carbonation resistance) contributes to the cost-efficient conservation of structures and helps meet sustainable development goals. It consequently spurs the circular economy, which aims to extend structures' service life and valorise the waste generated in their demolition as new raw materials.

One of the primary decay processes to which reinforced concrete structures are exposed is steel corrosion, traditionally deemed to comprise two periods, according to the Tuutti model [7]: an *initiation period* in which the aggressive agent penetrates into the concrete to the reinforcement depth and a *propagation period*, when corrosion begins. The most important causes of such decay are chloride penetration and concrete carbonation. Although the former is deemed to be the more aggressive of the two, inasmuch as two-thirds of all concrete structures are exposed to environments propitious to carbonation [8], the importance of understanding the process cannot be overlooked.

Carbonation, the result of the physical-chemical interaction between CO_2 in the atmosphere or dissolved in aggressive water [9] and the calcium phases in concrete, reduces alkalinity in the material to pH levels of under 9, favouring reinforcement depassivation [10,11]. The phases primarily involved in carbonation are calcium hydroxide (CH) and calcium silicate hydrates (C-S-H gel).

* Corresponding authors.
E-mail addresses: isaezdelu@unex.es (I.F. Sáez del Bosque), cmedinam@unex.es, cemedmart@yahoo.es (C. Medina).

https://doi.org/10.1016/j.conbuildmat.2019.117336
0950-0618/

Based on thermodynamic theory [12], CH should carbonate more readily than C-S-H gel. Empirical evidence shows, however, that carbonation may take place in the two phases simultaneously [13,14]. The process is affected by a number of factors [15–18], including degree of concrete saturation, water/cement ratio, cement content, mineral additions, aggregate type, curing time, porosity, CO_2 concentration, relative humidity and temperature.

Interest in the effect of recycled aggregates on CO_2 diffusion has been growing in the research community over the last 10 years, since in pursuit of a circular economy, the inclusion in concrete of construction and demolition and fired clay-based waste as coarse aggregate has become routine practice. The issue is of particular prominence in countries or regions where legislation, geography or availability of natural resources have necessitated the use of alternative raw materials [19].

The research conducted to date has focused on recycled concrete aggregate, with only a few papers published on fired clay-based and mixed recycled materials. Most of the literature on the subject shows that carbonation in materials with crushed concrete aggregate reaches depths 1.3- to 3.2-fold greater than in conventional concretes [16,18,20]. That difference is associated with the intrinsic properties (water absorption, density and porosity) of the recycled product, which raise permeability and water absorption in the host concretes [21,22]. Where recycled aggregate concrete (<30%) has been observed to behave similarly to the conventional material [23,24], those findings have been attributed to the low water/cement ratios in the new concretes or even deemed anomalous due to the small number of samples tested [24]. Those observations are consistent with the reliability-based analysis of recycled concrete exposed to carbonation conducted by Faleschini et al. [25], which showed that the water/cement ratio is the parameter with the highest impact on carbonation resistance in recycled aggregate concrete, with a much more significant effect than the aggregate replacement ratio.

The results reported for carbonation resistance in concrete bearing fired clay-based aggregate vary. Behaviour is similar to that of conventional concrete when <25% of the natural coarse aggregate is replaced by recycled sanitary ware industry waste aggregate [26,27]. Carbonation resistance is higher in materials bearing 20% to 100% masonry rubble waste [28] than in those with natural aggregate for two reasons. As the former require more cement to ensure mechanical performance they have a higher alkaline reserve, which protects the concrete surface against carbonation. The cement paste containing calcium hydroxide in the mortar adhered to recycled aggregates, in turn, may further increase the alkaline reserve in recycled concretes. That reserve is smaller, however, when the concrete contains fine aggregate from fired clay block and sanitary ware waste, which reduce the store of alkalinity because the fraction under 63 μm exhibits pozzolanic activity [29].

Carbonation in concretes containing both mixed recycled coarse aggregate and fired clay-based construction and demolition waste (bricks, sanitary ware, tiles and other ceramic materials) as a supplementary cementitious material is an innovative line of international research for a number of reasons. Firstly, there is a paucity of prior research on the simultaneous use of such waste, and only one study (authored by Bravo [30]) focused on concrete bearing 10% to 100% mixed recycled aggregate containing 69.1 wt% to 83.7 wt% mortar, concrete and unbound aggregate and 0.9 wt% to 28.6 wt% clay materials. That author reported carbonation depths 1.07 to 2.20 times greater than in the conventional material, depending on the replacement ratio and recycled aggregate composition. Secondly, research has yet to be published on the valorisation of the mixed ceramic fraction of construction and demolition waste (C&DW) as an addition in low-clinker cement design. Thirdly, the reuse of such waste is not addressed in the legislation on structural concrete manufacture, which restricts recycled aggregate to crushed concrete, envisaging replacement ratios of 20%, 25%, 30% or 100% depending on the the application and strength and target exposure class stipulated in the respective national legislation [31]. Fourthly, the industry generates vast amounts of mixed recycled waste, accounting for 67% of the recycled aggregate processed in Spain [32]. Fifthly, scientific understanding of carbonation and the prediction of the service life of these new materials is needed to ensure that the reinforcement remains passive throughout concrete service life. Sixthly, as no internationally published research has been conducted to date on the combination of newly patented cements (ref. ES2512065 [33]) with the coarse fraction of mixed aggregate, exploration of those conditions can make a significant contribution to the reuse of such waste in construction.

This study constitutes further research into CO_2 diffusion in concrete bearing 25% and 50% mixed recycled aggregate in which the binder is either OPC or cement containing 25% fired clay-based waste. The trials conducted to that end include phenolphthalein spray testing and instrumental techniques such as differential thermal and thermogravimetric analysis (DTA/TG), X-ray diffraction (XRD) and Fourier transform infrared spectroscopy (FTIR). Tensile strength, weight and porosity in concrete exposed to accelerated carbonation are also monitored. Service life is modelled based on CO_2 penetration using the procedure set out in Spain's structural concrete code.

2. Materials and methods

2.1. Materials

* The crushed graywacke natural aggregate used comprised three particle sizes: 12 mm to 22 mm, 6 mm to 12 mm and 0 mm to 6 mm. The mineralogy of this siliceous (SiO_2 > 60%) material consisted primarily of quartz, feldspars and phyllosilicates.

* The mixed recycled aggregate used, supplied by a construction and demolition waste plant located in the Spanish region of Extremadura, had two particle size fractions: 12 mm to 22 mm and 6 mm to 12 mm. It contained concrete and unbound aggregate (≈88 wt%), fired clay-based waste (≈10 wt%) and minor amounts of bituminous matter and floating particles. Its chemical constituents included SiO_2, Al_2O_3 and Fe_2O_3 (>60 wt%) and smaller percentages of other oxides. Quartz, potassium feldspars and plagioclase, along with chlorite, hematite and calcite, were the mineralogical phases detected.

The physical and mechanical properties of the coarse aggregates used are given in Table 1.

* The C&DW-sourced ceramic waste (CW) consisted of a mix of blocks, tiles, sanitary ware and other types of fired clay waste. An analysis of its chemical composition revealed the presence of SiO_2 (60 wt%), Al_2O_3 (19 wt%), Fe_2O_3 (6 wt%) and other minority oxides. The reactive silica content in this CW was greater than the 25% required for natural pozzolans as per European standard EN 197-1 [37], whilst the sum of the SiO_2, Fe_2O_3 and Al_2O_3 present was over the 70% specified in US standard ASTM C618-12 [38]. It exhibited a Blaine specific surface of 573 m^2/kg and density of 2.54 g/cm^3. The particle size distribution showed that 22.03% of the sample passed through the 10 μm sieve, 53.78% through the 50 μm sieve and 100% through the 90 μm sieve. The crystalline phases identified by the mineralogical analysis included quartz, phyllosilicates, feldspars, anorthite, calcite and hematite as crystalline phases.

* The following cements were used: CEM I 42.5R [37] ordinary portland cement (OPC) supplied by Lafarge, a cement manufacturer sited in the Spanish province of Toledo; and cement OPC + CW containing OPC and the CW mentioned above as a supplementary

Table 1
Physical and mechanical properties of coarse aggregates.

Characteristic [standard in References]	Natural aggregate		Recycled mixed aggregate	
	12/22 mm	6/12 mm	12/22 mm	6/12 mm
Real density of dry samples (kg/m^3) [34]	2.74	2.74	2.45	2.42
Water absorption (wt%) [34]	0.78	0.88	5.27	6.28
Flakiness index (wt%) [35]	25	21	10	10
Los Angeles coefficient (wt%) [36]	18	16	36	32

cementitious material. The latter cement, labelled OPC + CW, was prepared on a pilot scale and contained a blend of 75% OPC and 25% CW. This cement is registered under patent No. ES2512065 [33]. On the grounds of its physical, chemical and mechanical properties, it may be classified as a CEM II/B 42.5R or CEM IV/A 42.5R cement [39].

* A commercial polycarboxylate superplasticiser was added to the mixes (Bryten NF, supplied by FUCHS Lubricantes, S.A.U., Barcelona, Spain).

2.2. Concrete design

The six types of concrete prepared for this study were: the reference concrete (NC), made with OPC; reference concrete made with OPC + CW (RRC); concrete with OPC and 25% mixed recycled aggregate (NC-25); concrete made with OPC + CW and 25% mixed recycled aggregate (RRC-25); concrete with OPC and 50% mixed recycled aggregate (NC-50); concrete made with OPC + CW and 50% mixed recycled aggregate (RRC-50). Those ratios are higher than allowed by the legislation in place in France, Germany, Hong-Kong, Italy, Portugal, South Korea, Spain and United Kingdom for crushed recycled concrete aggregate in structural concrete requiring strength of over 25 MPa.

The concretes were batched as specified in the DOE British Method [40] to obtain a characteristic strength of 30 MPa at an effective w/c ratio of 0.45 and to ensure all the materials prepared had the same granular skeleton (Fig. 1).

The amount of water added in each mix was adjusted to take into account the water absorption of the granular skeleton (natural + recycled aggregate). To ensure a fluid consistency (100 mm-150 mm slump) the concretes containing recycled aggregate were mixed approximately 4 min longer than the materials with 100% natural aggregate with a view to gradual water absorption by the recycled aggregate.

Concrete mix design, slump and 28 d compressive strength [41] are given in Table 2.

The mixes designed met the minimum cement ($\geq$275 kg/m^3) and maximum effective w/c ratio ($\leq$0.60) requirements laid down in both Spain's structural concrete code (EHE-08) [3] for concretes in carbonation-induced corrosion exposure classes IIa and IIb and European standard EN 206 [1] for exposure classes XC1, XC2, XC3 and XC4.

2.3. Pre-conditioning and experimental procedure

Cylindrical specimens (100 $\phi \times$ 200 h mm, Fig. 2) were cured for 28 d in water, followed by standardised pre-conditioning consisting in drying at 40 °C for 1 week and subsequent sealing with steam-proof polyethylene and storage at 20 °C and RH = 60% for 3 weeks. After conditioning (Fig. 2), three samples per mix were tested for splitting tensile strength (t = 0 d); three samples per mix were stored in a climate chamber at 20 °C and 60% RH for 56 d, after which they were vacuum-saturation tested as described in standard NBN B 05-201 [42]; and 15 samples per mix were subjected to accelerated carbonation for 14 d, 28 d, 42 d or 56 d.

The vacuum saturation procedure consisted in placing the specimens in a tank at a residual pressure of 2.7 kPa. After 2.5 h, water was added at a rate of 50 mm/h until the specimens were completely immersed. The air pressure was subsequently restored and the cylinders were kept under water for 24 h. The specimen mass was measured under water (m_2) in dry saturated surface conditions (m_3) and after drying in an oven at 40 °C for 14 days to a constant mass (dry mass, m_1).

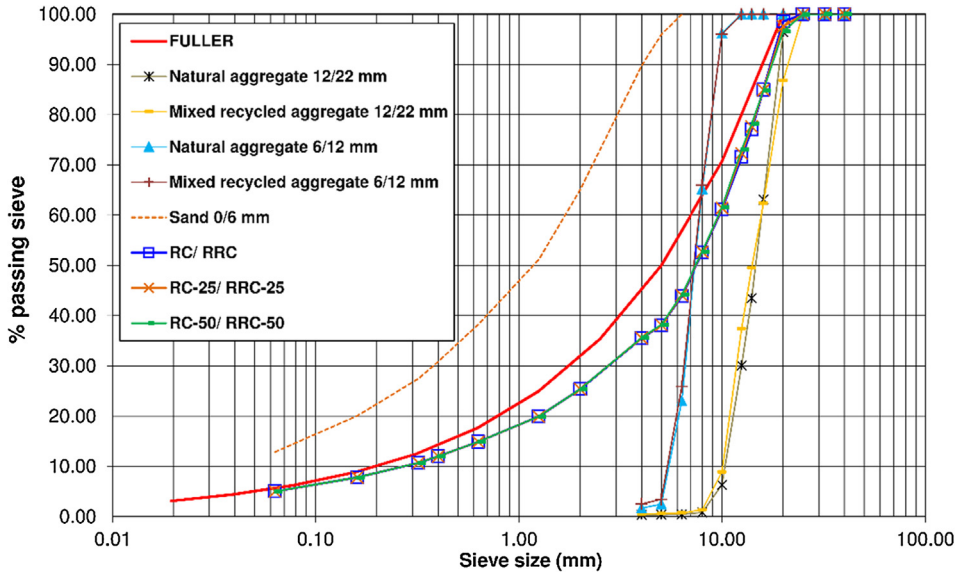

Fig. 1. Particle size distribution curves for the mixed aggregates used in the concretes designed.

Table 2
Concrete mix design, slump and compressive strength.

Material	Mixture					
	NC	NC-25	NC-50	RRC	RRC-25	RRC-50
A (kg/m^3)	732.4	720.8	705.4	732.4	720.8	705.4
B (kg/m^3)	766.7	565.9	369.2	766.7	565.9	369.2
C (kg/m^3)	383.0	282.7	184.4	383.0	282.7	184.4
Brc (kg/m^3)	–	182.8	357.8	–	182.8	357.8
Crc (kg/m^3)	–	90.7	177.6	–	90.7	177.6
Water (kg/m^3)	193.0	202.1	210.6	193.0	202.1	210.6
OPC (kg/m^3)	400.0	400.0	400.0	–	–	–
OPC + CW (kg/m^3)	–	–	–	400.0	400.0	400.0
SP (kg/m^3)	6.2	6.2	6.2	6.2	6.2	6.2
(w/c) $_{effective}$	0.45	0.45	0.45	0.45	0.45	0.45
Property						
Slump (mm)	110	120	130	110	130	130
fc (MPa)	51.16 ± 0.18	51.69 ± 0.65	51.16 ± 0.58	46.06 ± 0.60	45.71 ± 1.41	41.18 ± 0.10

Note. – *In this batching method the total (coarse + fine) aggregate volume depends on fresh concrete density. That, in turn, depends on the mean density of the granular skeleton (and hence on the replacement ratio) and the effective water content.
A: natural sand (0/6 mm); B: natural gravel 1 (12/22 mm); C: natural gravel 2 (6/12 mm); Brc: recycled gravel 1 (12/22 mm); Crc: recycled gravel 2 (6/12 mm); OPC: ordinary portland cement; OPC + CW: cement containing SCMs from construction and demolition waste; SP: superplasticiser; CS: 28 d compressive strength of 150x150x150 mm^3 cubic specimens

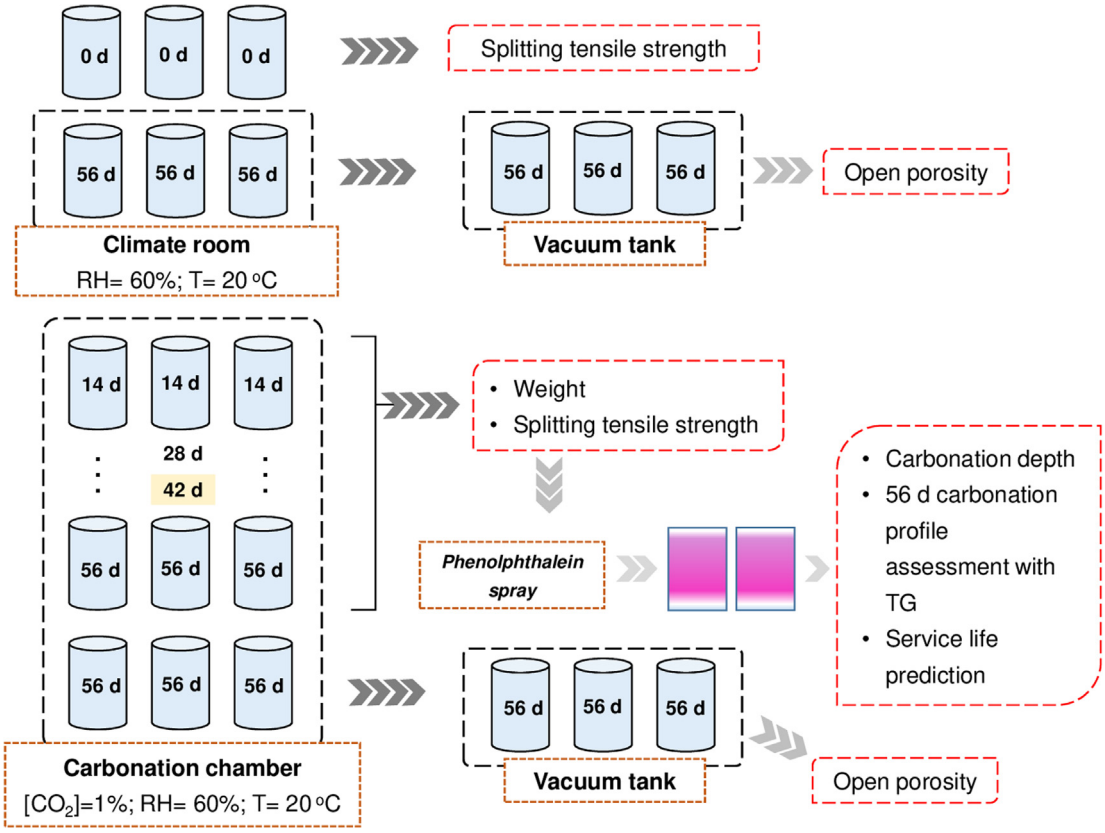

Fig. 2. Experimental procedure (0 time = 28 d of curing + 1 week at 40 °C + 3 weeks of storage at 20 °C and 60% RH).

Open porosity (porosity accessible to water) (φ) was calculated from Eq. (1):

$$\varphi = [(m_3 - m_1)/(m_3 - m_2)] \times 100 \quad (1)$$

2.4. Accelerated carbonation test

CO_2 permeability was determined with the accelerated carbonation method described in Spanish standard UNE 83993-2 [43], in which carbonation penetration in concrete is accelerated in a chamber with a CO_2 concentration of 1%, a temperature of 20 °C and a relative humidity of 60 ± 5%.

The specimens were monitored for carbonation depth and subsequently weighed. Splitting tensile strength tests were conducted after exposure for 14 d, 28 d, 42 d or 56 d (Fig. 2).

2.5. Carbonation monitoring techniques

2.5.1. Phenolphthalein spray test and carbonation depth

Carbonation depth was determined with the colorimetric test set out in Spanish standard UNE 112-011 [44]: two sides of the

specimens resulting from the splitting tensile strength test were sprayed with 1% phenolphthalein in a 70% alcohol solution. Phenolphthalein is pinkish-fuchsia at pH values of over 10, where samples are uncarbonated, and colourless at values of under 8, denoting carbonation. A total of 12 measurements were taken longitudinally and three diametrically at the top of the specimen. The mean value of the 15 measurements was then calculated, along with the maximum and minimum penetration depths.

2.5.2. Carbonation coefficient

Carbonation depth is generally deemed to increase with the square root of time in the proportion defined by the carbonation coefficient. That relationship, used to estimate how long it takes the carbonation front to reach the reinforcing steel bars and trigger depassivation [18], is based on Ficks first law, as follows (Eq. (2)):

$$d(t) = d_0 + K_{field}\sqrt{t} \tag{2}$$

where $d(t)$ is the carbonation depth at time = t (mm), d_0 is the carbonation depth at time = 0 (mm), K_{field} is the carbonation coefficient (mm/year$^{0.5}$) and t is the time in service or exposure time (years).

Eq. (3), which gives the ratio of the accelerated (K_{acce}) and field (K_{field}) carbonation coefficients in terms of their respective CO_2 concentrations, c_{acce} (1%) and c_{field} (0.04%), was applied to find the carbonation coefficients under atmospheric conditions [18,45,46].

$$K_{field} = \frac{K_{acce}\cdot\sqrt{c_{field}}}{\sqrt{c_{acce}}} \tag{3}$$

2.5.3. Differential thermal (DTA) and thermogravimetric (TG) analysis

The 56 d cylindrical specimens were analysed with DTA and TG. Powder was obtained with a 10 mm diameter diamond bit, drilling along an 180 mm long, 20 mm wide region to ensure that the powder was representative and at the following depths from the surface exposed to CO_2: 0 mm to 1.0 mm (layer 1); 1.5 mm to 3.5 mm (layer 2); 4.0 mm to 6.0 mm (layer 3); 6.5 mm to 7.5 mm (layer 4); and 8.0 mm to 10.0 mm (layer 5). After removal the powder samples were vacuum-dried to detain hydration.

DTA/TG readings were taken with an SDT Q600 analyser on approximately 70 mg of powder heated from 20 °C to 1000 °C at 10 °C/min in nitrogen flowing at 100 mL/min. The initial and final temperatures for the portlandite (CH) dehydroxylation and calcium carbonate (CC_t) decomposition reactions, determined from the first derivative of weight loss vs temperature curve (DTG), together with mass loss from TGA, were used to estimate the amount of CH and CCt present in each sample. Mass loss, obtained from the TG curve using the tangential method, is expressed in percent of initial weight.

The loss of CO_2 attributable to CC_t decomposition was governed by the equation: $CaCO_3$ (s) → CaO (s) + ↑CO_2 (g). The temperature range for that loss is normally deemed to run from the end of CH decomposition (460 °C) through to 900 °C to 950 °C. The total calcium carbonate content (CC_t) was consequently found as the percent of mass loss due to CC_t decomposition as determined by TGA (WL_{CCt}) multiplied by molecular mass ratio (M_{CCt}/M_{CO_2}), as per Eq. (4):

$$CCt(wt\%) = WL_{CCt}\times\frac{M_{CC}}{M_{CO_2}} = WL_{CCt}\times\frac{100}{44} \tag{4}$$

The carbonate content attributable solely to CO_2 exposure (carbonation) was determined by calculating the amount in wt% of CC_t in the carbonated sample, CCt (i = 56 d), less the initial content in wt% in the uncarbonated sample, CCt^0:

$$CCt_c(wt\%) = CCt^i(wt\%) - CCt^0(wt\%) \tag{5}$$

When CH decomposes (generally between 410 °C and 480 °C) in CaO and H_2O, the mass loss recorded is due to the loss of water. The amount of CH was therefore determined as the percent of mass loss due to CH dehydroxylation (WL_{CH}) found with TGA multiplied by the molecular mass ratio (M_{CH}/M_{H_2O}) as per Eq. (6):

$$CH(wt\%) = WL_{CH}\times\frac{M_{CH}}{M_{H_2O}} = WL_{CH}\times\frac{74}{18} \tag{6}$$

2.5.4. X-ray diffraction

The powder removed from the 56 d carbonated specimens was used in XRD analysis, conducted on a Bruker D8 Advance X-ray diffractometer fitted with a 3 kW copper anode (Cu-K$\alpha_{1,2}$). The running conditions were 40 kV and 30 mA, the count time per step was 31.5 s and the step size 0.019°. Measurements were recorded for a 2θ angular range of 5° to 60°.

2.5.5. Fourier transform infrared spectroscopy (FTIR)

Fourier transform infrared (FTIR) spectra were recorded with a Nicolet 6700FTIR spectrometer over a range of 4000 cm^{-1} to 400 cm^{-1} on pellets prepared by mixing 1 mg of sample with 300 mg of KBr. This technique was deployed to determine the type of calcium carbonate polymorphs formed during carbonation.

2.6. Service life prediction

The durability limit state associated with carbonation-induced reinforcement depassivation [4] can be defined as in Eq. (8) (EHE-08 [3]):

$$t_L > t_d > \gamma_f\cdot t_{SL} \tag{8}$$

where t_L is the estimated service life, t_d the design value of the service life, t_{SL} the design service life depending on the type of structure (monumental or emblematic buildings, bridges and other civil structures with a high economic impact) in years (=100 years) and γ_f the safety factor for service life, which takes a value of 1.10.

Characteristic depth $x_{c,c}$ can be found with Eq. (9) (from the CO_2 design penetration model in EHE-08 [3]).

$$x_{c,c}(t_{SL}) = K_{field}\sqrt{t_d} = K_{field}\sqrt{\gamma_f\cdot t_{SL}} \tag{9}$$

where γ_f is the safety factor for service life described in Eq. (8) (γ_f = 1.10 in EHE-08).

3. Results and discussion

3.1. Mechanical behaviour of concrete

Splitting tensile strength at the beginning of the test (CO_2 exposure time, 0 d) and its fluctuation during exposure to carbonation are given in Table 3.

Table 3. Concrete splitting tensile strength (N/mm^2 = MPa) before and during exposure to CO_2

The inclusion of cement with recycled contents (OPC + CW) induced a 3.6% loss in initial strength in RRC relative to NC, a 2.2% loss in RRC-25 relative to NC-25 and a 1.7% loss in RRC-50 relative to NC-50. The inclusion of 25% mixed recycled aggregate, irrespective of cement type, was observed to have no adverse effect on mechanical performance, whilst the addition of 50% induced a loss of under 3.7% relative to the reference. The differences were not statistically significant ($p > 0.05$). Such good mechanical performance was directly related to the intrinsic properties of the recycled aggregate/paste ITZ. Earlier research [47,48] on the properties of the recycled aggregate/paste ITZ in concretes with 25% fired clay sanitary ware or 50% mixed recycled coarse aggregate (concrete, fired clay materials, plastic...) showed that the fired clay-base aggregate/paste ITZ behaved better than the natural aggregate/paste ITZ. According to the same studies, the performance of the newly

Table 3
Concrete splitting tensile strength (N/mm^2 = MPa) before and during exposure to CO_2.

Concrete mix	Exposure time CO_2 (days)				
	0*	14	28	42	56
NC	4.14 ± 0.27	4.36 ± 0.22	4.61 ± 0.45	4.91 ± 0.24	5.03 ± 0.16
NC-25	4.13 ± 0.15	4.48 ± 0.09	4.54 ± 0.32	4.99 ± 0.42	5.13 ± 0.14
NC-50	3.99 ± 0.22	4.22 ± 0.10	4.26 ± 0.08	4.58 ± 0.14	4.78 ± 0.18
RRC	3.99 ± 0.25	4.32 ± 0.36	4.50 ± 0.27	4.80 ± 0.40	4.88 ± 0.02
RRC-25	4.04 ± 0.10	4.47 ± 0.22	4.68 ± 0.19	4.90 ± 0.30	5.12 ± 0.15
RRC-50	3.92 ± 0.10	4.10 ± 0.31	4.21 ± 0.31	4.38 ± 0.21	4.63 ± 0.14

* Specimens cured for 28 d and preconditioned as described in Section 2.3 prior to exposure to CO_2.

formed ITZ between the old recycled concrete aggregate and the new cement matrix was similar to that of the natural aggregate/-paste ITZ.

In all the materials studied, tensile strength rose faster than expected with exposure time due to carbonation, primarily affecting the portlandite present in the outer layers. The strength rise when exposed to carbonation amounted to 18% to 27%, which is more than the 8% to 15% strength increase observed when the concretes were exposed to real conditions. That behaviour might be associated with the effect of carbonation on the microstructure, which translated into pore system refinement and a decline in total porosity [49,50] (Table 6). The precipitation of many small rhomboid crystals, products of the reaction between CH and CO_2, lessened the change in the microstructure.

3.2. Carbonation depths

3.2.1. Mean depth

Fig. 3 shows that mean carbonation depth rose with exposure time in the concretes tested and that the standard deviation calculated for each trial was lower than the mean 15% carbonation depth. At all ages, the concretes made with conventional cement (NC, NC-25 and NC-50) exhibited greater resistance to CO_2 penetration than the concretes with cement containing supplementary cementitious materials (OPC + CW), with increases in the 56 d mean depth of +0.92 mm in RRC relative to NC, +1.10 mm in RRC-25 relative to NC-25 and +1.05 mm in RRC-50 relative to NC-50.

Those slight rises were due primarily to the lower portlandite content resulting from the pozzolanic reaction mediated by the addition of clay-based materials (tiles, bricks...) from C&DW in the cement, as well as from the dilution of the clinker content due to cement replacement. The presence of a smaller amount of portlandite available to react with the CO_2 gas lowered the buffering capacity and hence raised the speed of CO_2 penetration [51]. Ekolu [17] contended that in concretes made with cements containing SCM replacements, that difference is not associated solely with the dilution associated with the smaller amount of clinker. A second effect is attributable to the longer curing time generally required by these new cements in comparison with CEM I: if curing is insufficient, the pozzolanic reaction that fills pores is often absent (depending on the addition).

That reasoning is consistent with other authors' findings in connection with pozzolans such as silica fume [52], fly ash [53] and ground granulated blast furnace slag [54], with rises in carbonation depth of 1.7 mm to 5.5 mm for replacement ratios of 10% in SF (accelerated testing; 20 week exposure; 3.5% CO_2; 20 °C; 60% RH) and 25% in FA and GGBFS (natural testing; 10 year exposure).

Fig. 3 also shows that the inclusion of mixed recycled aggregate deepened CO_2 penetration, an effect that was intensified with rising replacement ratios. In the 56 d carbonated materials, penetration was +0.49 mm deeper in NC-25 and +0.90 mm in NC-50 than in NC; and +0.67 mm deeper in RRC-25 and +1.02 mm in RRC-50 than in RRC.

Consequently, after 56 d the carbonation front was 1.10 times deeper in the concretes with 25% recycled aggregate (NC-25 and

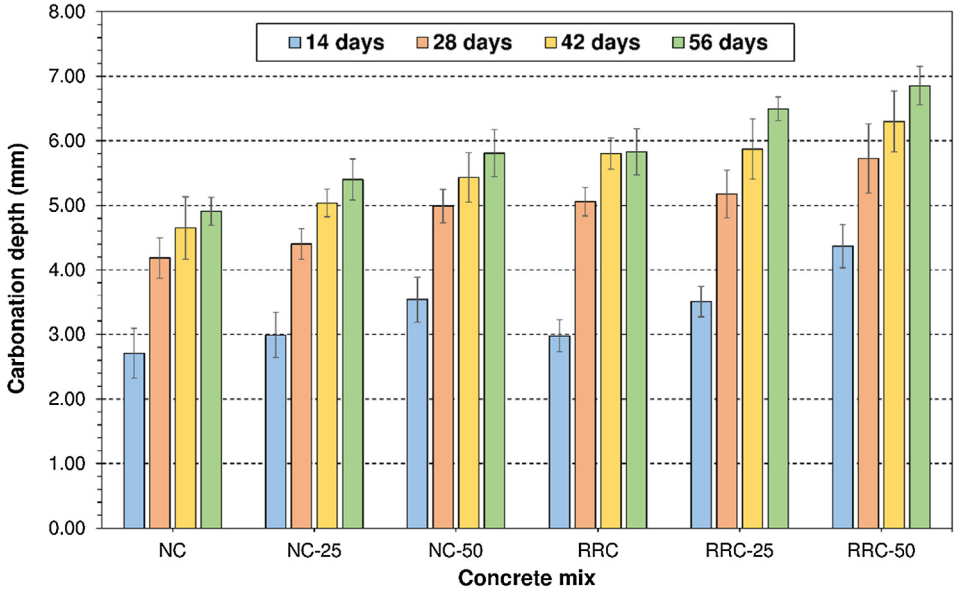

Fig. 3. Fluctuations in mean carbonation depth.

RRC-25) and 1.18 times deeper in the materials with 50% RCA (NC-50 and RRC-50) than in the concretes with 100% natural aggregate. Those values were very close to reports by Bravo et al. [30] for concretes with mixed recycled aggregate (1.07 to 1.42 times deeper in case of 25% replacement and 1.21 to 1.68 times in case of 50% replacement compared to the reference, depending on the composition of the recycled material). They were likewise similar to the increases observed by other authors for recycled concrete aggregate (1.10 to 1.19 times for 25% [55,56], 1.17 to 1.75 times for 50% [56,57] and 2 to 2.3 times for 75% to 100% replacement [56,58] relative to conventional concrete). The BCSJ guide [59], in turn, cites increases of 1.2 to 2 times the conventional concrete values.

The rise observed for the simultaneous use of cement with recycled contents and mixed recycled aggregate was similar to but lower (1.08 times compared to 1.37 to 1.71 times) than found by Kou et al. [53], Faella et al. [60] and Xiao et al. [61] for concretes containing fly ash (25%, 30% and 10%), slag (10%) or silica fume (10%) -additioned cement and recycled concrete aggregate (50%, 60% and 100% replacement in [46,53,54] respectively) exposed to natural carbonation.

The relationship between penetration and the presence of recycled aggregate was linear with a determination coefficient (R^2) of over 0.85, irrespective of exposure time and type of cement used, as shown by the data in Table 4.

The lower resistance to carbonation in the concretes with recycled aggregate than in those with natural aggregate is associated with a number of factors. A first group includes the intrinsic characteristics of recycled aggregate, such as greater permeability [62], water absorption [51,63], and porosity [53,64], greater and pore water retention [51,52] and, to a lesser extent, the possible presence of microcracks as a channel for CO_2 penetration in the old ITZ (aggregate/paste) [30] due to the primary and secondary crushing involved in material processing. A second factor comprises the intrinsic properties of these new recycled concretes, particularly their greater permeability (Section 3.4) attributable to their greater porosity (due to the greater porosity of recycled than natural aggregate) than found in conventional concretes, as observed in earlier reports [7,17,65].

The graph in Fig. 4 plotting splitting tensile strength against CO_2 penetration shows that inasmuch as the area affected by carbonation in the concretes studied was small, tensile strength rose with penetration depth (more than when the materials were exposed to natural conditions) and the two parameters were linearly related with a correlation coefficient of over 0.83. That pattern was directly related to the changes in the pore fraction of concrete during carbonation (see 3.4). Similar behaviour was observed by Singh and Singh [66], who calculated an R^2 of over 0.80 for the linear correlation between carbonation depth and the compressive strength of self-consolidating concrete bearing recycled concrete (coarse and fine) aggregate and binary (OPC + fly ash or silica fume) or ternary (OPC + metakaolin + fly ash) cement. R^2 values of > 0.80 are indicative of overall satisfactory performance.

3.2.2. Maximum and minimum depth

As the charts in Fig. 5a) and b) show, irrespective of the type of cement used and exposure time, the highest values for the maximum and minimum carbonation depth in recycled concrete were recorded for the materials with the higher replacement ratio (NC-50 and RRC-50). Note that as specified in the following paragraph and in European standard prEN 12390-12, the maximum depths were not included in mean depth calculations.

The maximum depth was observed where the penetration front was interrupted either (primarily) by a recycled aggregate particle or by an air pore. Pursuant to the provisions of European standard prEN 12390-12 [67], those values were excluded from mean carbonation depth calculations.

The carbonation fronts (colourless areas) for concretes RRC-50 and NC-50 depicted in Fig. 6 exhibited similar forms, an indication that CO_2 diffusion was uniform and unaffected by the inclusion of recycled aggregate or cement type.

3.2.3. Statistical significance of cement type and aggregates in carbonation depth

The ANOVA showed that when acting separately, all three factors, i.e., recycled aggregate content, cement type and exposure time, had a significant effect (p-value < 0.05) on mean carbonation depth, whereas the interaction among them did not significantly impact that dependent variable (p-value > 0.05).

The model explained 84% of the variation observed in carbonation depth (the dependent variable). As Fig. 7 shows, the factor explaining the largest percentage of variation was exposure time (≈64%), followed by cement type (≈11%) and mixed recycled aggregate (≈6%). Those findings support the results discussed in item 3.2.1, according to which these three factors had a significant effect on mean carbonation depth. The above data were also consistent with a study by Guo et al. [20], who observed that the aforementioned factors had an adverse effect on carbonation resistance in concrete made with recycled crushed concrete aggregate.

The statistical models obtained for the concrete families studied (with OPC, NC/NC-25/NC-50, or OPC + CW, RRC/RRC-25/RRC-50) further supported the significance of the effect of exposure time and recycled mixed aggregate on carbonation depth when acting separately (p-value < 0.05) and the absence of significance of their interaction (p-value > 0.05). These models explained 80% of the variation observed in CO_2 penetration, with no differences in the contribution of exposure time (≈70%), mixed recycled aggregate (≈7%) or ET*RMA (≈1%) (Fig. 7) between the two concrete families.

In addition, Tukey's HSD multiple range test conducted for carbonation depth in the concretes revealed the presence of two homogeneous groups in each family of concrete, OPC and OPC + CW. Moreover, the means for the two families differed significantly (p-value < 0.05). In both cases the inclusion of 50% recycled aggregate induced the most statistically significant effect on carbonation depth.

Table 4
Correlation between carbonation depth and mixed recycled aggregate replacement ratio.

Exposure time (days)	Type of cement					
	Conventional cement (OPC)			Recycled cement (OPC + CW)		
	a	b	R^2	a	b	R^2
14	0.02	2.66	0.968	0.03	2.92	0.981
28	0.02	4.12	0.934	0.01	4.98	0.878
42	0.02	4.65	1.000	0.01	5.74	0.852
56	0.02	4.92	0.997	0.02	5.88	0.971

Note. - y = ax + b, where: y is the carbonation depth; a is the slope of the line; b is a constant; x is the mixed recycled aggregate replacement ratio; and R^2 the correlation coefficient.

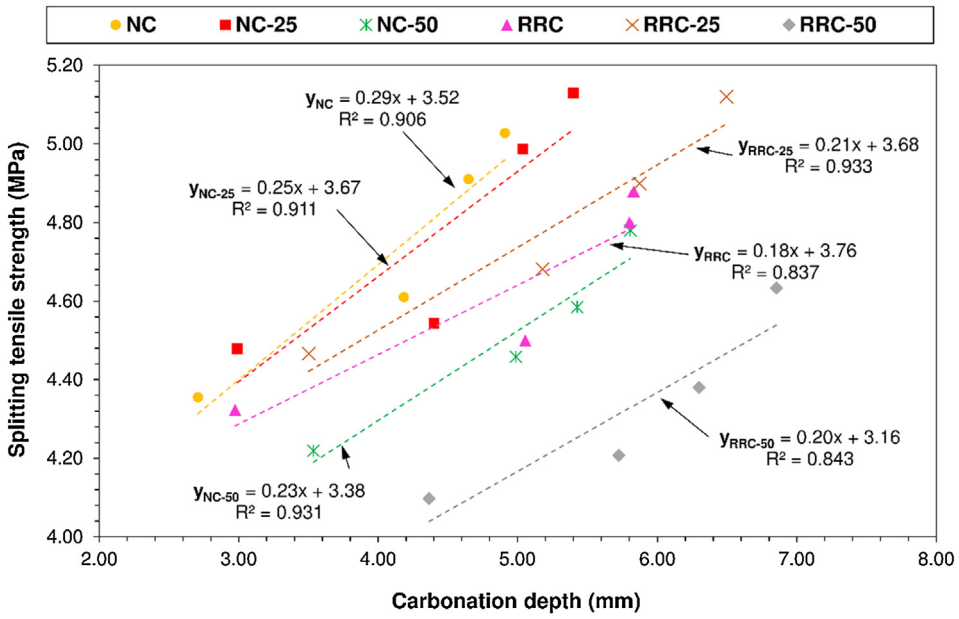

Fig. 4. Tensile strength vs carbonation depth.

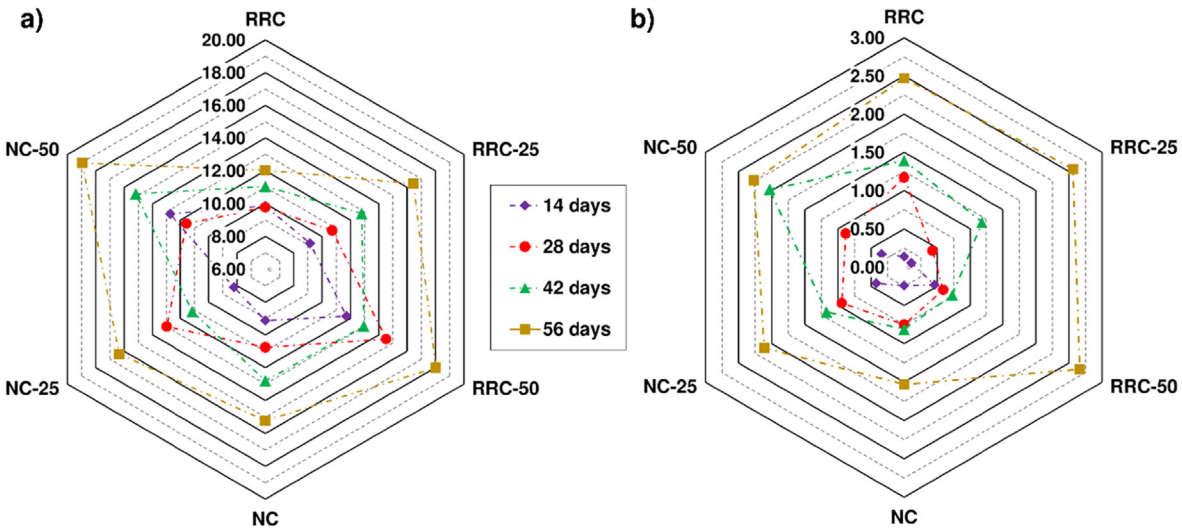

Fig. 5. Carbonation depth (in mm): a) maximum; b) minimum.

Conventional cement group 1 included two elements, NC and NC-25, meaning that their mean carbonation depths were not significantly different. Similarly, group 2 comprised concretes NC-25 and NC-50. Recycled cement concrete group 3, in turn, also had two members, RRC and RRC-25, whereas group 4 had only one, RRC-50. These findings showed that the inclusion of small percentages of mixed recycled aggregate (≤25%) induced no statistically significant change in concrete carbonation depth, irrespective of the type of binder used.

3.3. Carbonation coefficient

The carbonation depth vs square root of exposure time plots in Fig. 8 show that the relationship was linear in all the concretes tested (Equation (2)), with a determination coefficient of $R^2 > 0.97$.

The findings confirmed that carbonation took place more rapidly in the presence of mixed recycled aggregate and the cement OPC + CW than in the conventional material. The carbonation coefficient was 1.05 to 1.19 times larger in concretes with recycled aggregate (NC-25, NC-50, RRC-25 and RRC-50) relative to concretes with natural aggregate (RRC and NC) and proportional to the replacement ratio; it was also larger in concrete containing OPC + CW than in concrete made with OPC (1.20 times in concrete RRC relative to RC, 1.16 times in RRC-25 relative to NC-25 and 1.17 times in RRC-50 relative to NC-50). The linear relationship in concretes with conventional cement fit the equation $K_c = 0.05x + 13.48$ ($R^2 = 1.00$) and in concrete with recycled cement $K_c = 0.05x + 16.06$ ($R^2 = 0.99$), where K_c is the accelerated carbonation coefficient and x the mixed recycled aggregate replacement ratio.

Similar behaviour was observed by earlier authors. Faella et al. [60], studying fly ash and recycled concrete aggregate, found the carbonation coefficient in the new concretes to be 1.25 to 1.48 times greater than in the reference and to rise linearly with the percentage of recycled aggregate. Kou and Poon [53] reported 1.04-fold rises in the carbonation coefficient for concretes with 50% recycled concrete aggregate and of 1.14-fold in 25% fly ash

Fig. 6. 56 d carbonation front in specimens exposed to CO_2 at a concentration of 1%: a) RRC; b) NC; c) RRC-50; d) NC-50.

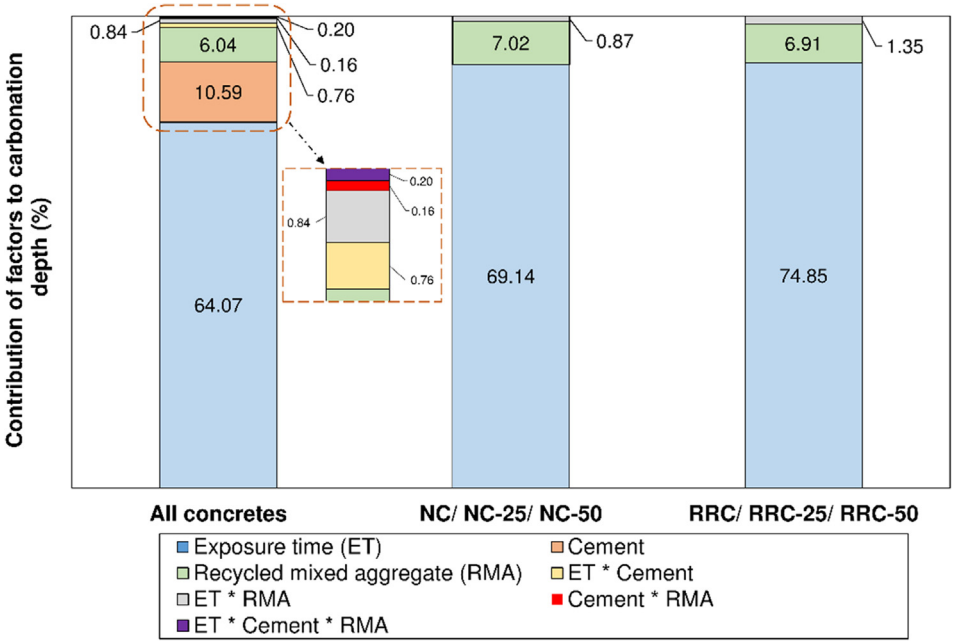

Fig. 7. Contribution of factors to variation in mean carbonation depth.

cement concretes with 50% recycled aggregate. Pedro et al. [64] observed the carbonation coefficient in concrete with 100% recycled aggregate to be 1.29 times greater than in the reference and to be linearly related to the replacement ratio ($R^2 > 0.87$).

The accelerated (K_{acce}) and real (K_{field}) carbonation coefficients resulting from applying Eq. (3) are compared in Table 5, in which atmospheric CO_2 concentration was assumed to be 0.04% [10]. All the values for K_{field} were less than the 4 mm/year$^{0.5}$ cited for conventional concretes in field conditions [68].

Based on the K_{field} values obtained and the classifications proposed [69,70] by authors from different countries, in which concrete quality is based on the carbonation coefficient under atmospheric conditions, all the concretes were of good quality (K_{field} < 5 mm/year$^{0.5}$): concretes NC-50, RRC, RRC-25 and RRC-50

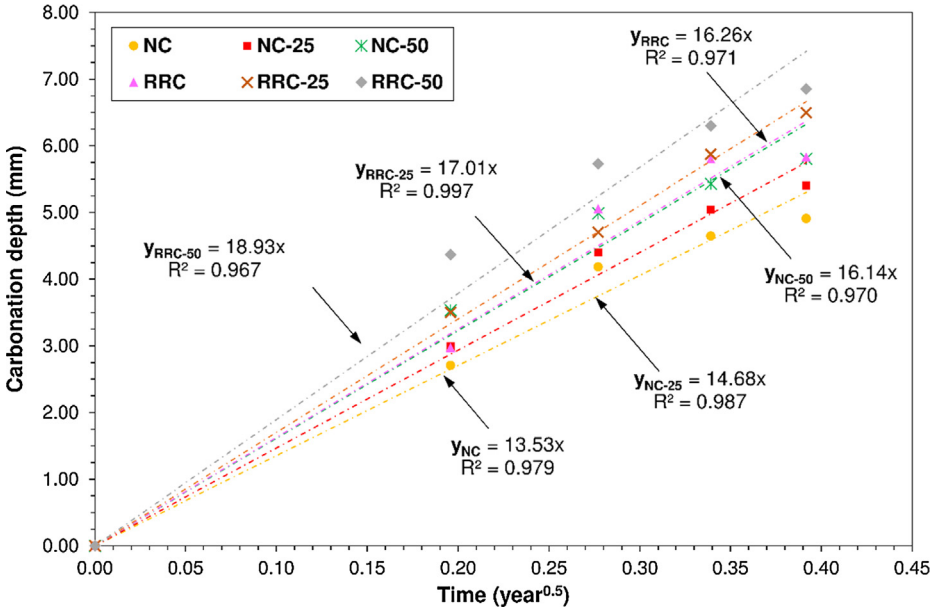

Fig. 8. Carbonation depth vs time$^{0.5}$ of exposure to CO_2.

of good (3 mm/year$^{0.5}$ < K_{field} < 6 mm/year$^{0.5}$) and concretes NC and NC-25 of high quality (K_{field} < 3 mm/year$^{0.5}$).

Likewise based on the carbonation coefficients under real conditions (K_{field}) and the classification proposed by Greve-Dierfeld and Gehlen [71], concretes NC and NC-25 lay within the range of resistance to carbonation class RC3 (2–3 mm/year$^{0.5}$) and the other materials within the class RC4 (3–4 mm/year$^{0.5}$).

3.4. Weight and open porosity

Weight gain in specimens exposed to accelerated carbonation for 14 d, 28 d, 42 d or 56 d is plotted against carbonation depth in Fig. 9. Irrespective of the concrete analysed, weight rose with exposure time, which was in turn related to increased carbonation depth. Weight gain and carbonation depth were linearly correlated with an R^2 > 0.86. Those data were the direct outcome of the changes in concrete pore structure caused by the calcium carbonate generated in the reaction between portlandite and atmospheric CO_2 (Table 6).

The open porosity for concretes after carbonation in the accelerated carbonation chamber and for the uncarbonated materials only cured in the climate chamber at a constant 20 °C and RH of 60% are given in Table 6. The decline observed in this parameter is normally associated with the 11% to 14% rise in carbonate molar volume relative to the reacted CH [72,73]. Nonetheless, C-S-H gel carbonation, which entails calcium ion leaching and the formation of amorphous silica gel, reduces the volume of solids and raises porosity [74,75]. Due to the stoichiometric variation (C/S ratio) involved [76], the change in the volume of solids taking place with C-S-H gel carbonation is not fully understood however, and is often calculated by establishing a fixed C/S ratio for the gel [13]. As these two opposed physical developments occur simultaneously, the reduction of open porosity observed here may be indicative of a more predominant role of CH than C-S-H gel carbonation. That inference would be consistent with the pattern observed by Gruyaert et al. [77] and Leemann [49], who reported a decline in porosity with exposure time in concretes with different percentages of blast furnace slag and additions such as fly ash, limestone and silica fume.

The data in Table 6 also showed that the relative decline in open porosity was similar for all concretes, although it rose slightly with rising recycled aggregate content.

The linear relationship (R^2 > 0.95) between open porosity and 56 d carbonation depth (Fig. 10) shows that open porosity and carbonation depth rose in all cement types when natural aggregates were replaced with recycled aggregates. This finding is consistent with reports by Vieira et al. [29] and Limbachiya et al. [52], who associated deeper carbonation primarily with concrete pore structure and more specifically with open porosity. The higher carbonation depths at the same open porosity values for the mixes with OPC + CW were attributable to their lower CH content, which reduced their buffering capacity.

Table 5
Accelerated and real carbonation coefficients.

Concrete mix	Carbonation coefficient (mm/year$^{0.5}$)	
	$K_{acce.}$	K_{field}
NC	13.53	2.71
NC-25	14.68	2.94
NC-50	16.14	3.23
RRC	16.26	3.25
RRC-25	17.01	3.40
RRC-50	18.93	3.79

3.5. DTA/TG, XRD and FTIR study of carbonation profiles

The DTG curves for the five layers analysed in the 56 d samples are reproduced in Fig. 11. Two or three signals were detected, depending on the layer:

i) 50 °C–390 °C: water loss due to C-S-H/AFt/AFm decomposition
ii) 390 °C–460 °C: water loss due to CH dehydroxylation
iii) 460 °C–950 °C: CO_2 loss associated with total carbonate (CCt) decomposition, with a moderate intensity peak at around 560 °C to 564 °C (CC_1), a high intensity peak at 700 °C to 748 °C (CC_2) and a low intensity peak at 860 °C to 879 °C (CC_3). Carbonate profiles with three peaks have been reported by only a few authors [13,14,78], who observed the signals at different intensities and temperature ranges.

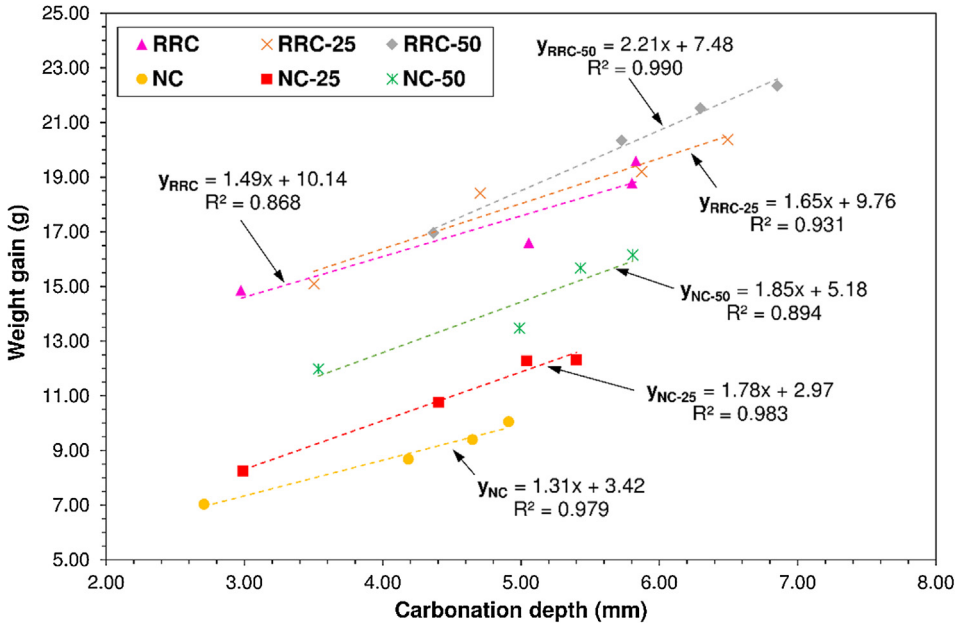

Fig. 9. Weight gain vs carbonation depth.

Table 6
Open porosity at the beginning and end of the exposure period.

Concrete mix	Open porosity (%)		
	Uncarbonated (from climate chamber)	56 d accelerated carbonation	Difference (%) climate room – 56 d carbonation
NC	6.85 ± 0.42	6.39 ± 0.21	−5.34
NC-25	7.68 ± 0.50	7.21 ± 0.32	−6.16
NC-50	9.33 ± 0.30	8.67 ± 0.25	−7.13
RRC	7.37 ± 0.55	6.94 ± 0.54	−5.86
RRC-25	9.60 ± 0.24	9.00 ± 0.19	−6.29
RRC-50	10.97 ± 0.34	10.10 ± 0.27	−7.90

Of the three calcium carbonate polymorphs, vaterite, aragonite and calcite, the third is the most thermally stable, decomposing at over 750 °C (in pure, perfect crystals [79]). Vaterite and aragonite are metastable at low temperatures and atmospheric pressure and convert irreversibly to calcite when heated [80], although vaterite may convert first to aragonite [81]. Conversion is associated with an endothermal event taking place at a temperature below the calcite decomposition temperature: for aragonite at ~402 °C to 500 °C [80,82] and for vaterite at ~450 °C to 600 °C [80,83]. According to Sauman et al. [84], vaterite decomposes into imperfectly crystallised calcite that exhibits a lower decomposition temperature (at approximately 700 °C) than pure calcite.

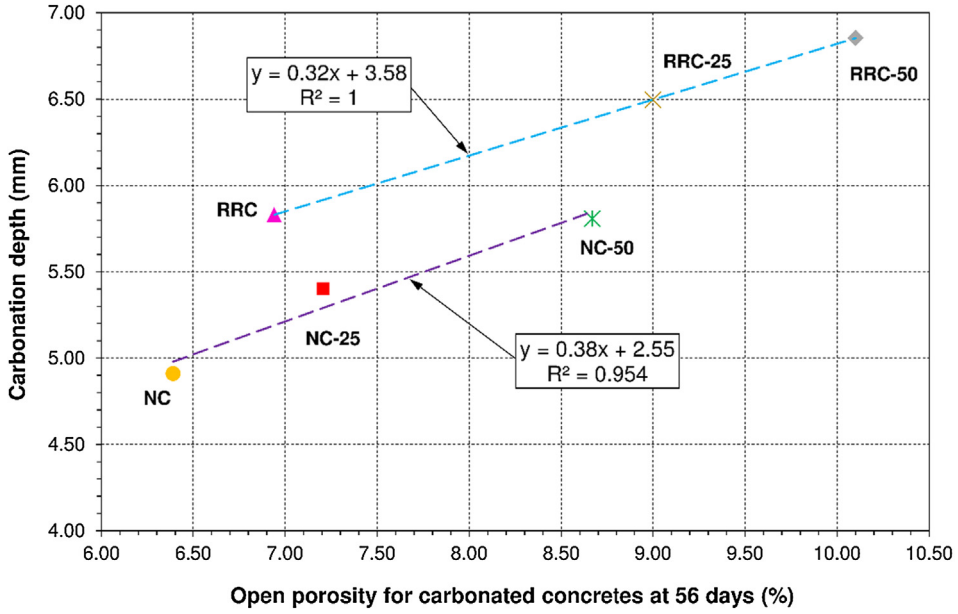

Fig. 10. Open porosity vs carbonation depth after 56 days carbonation at 1% CO_2.

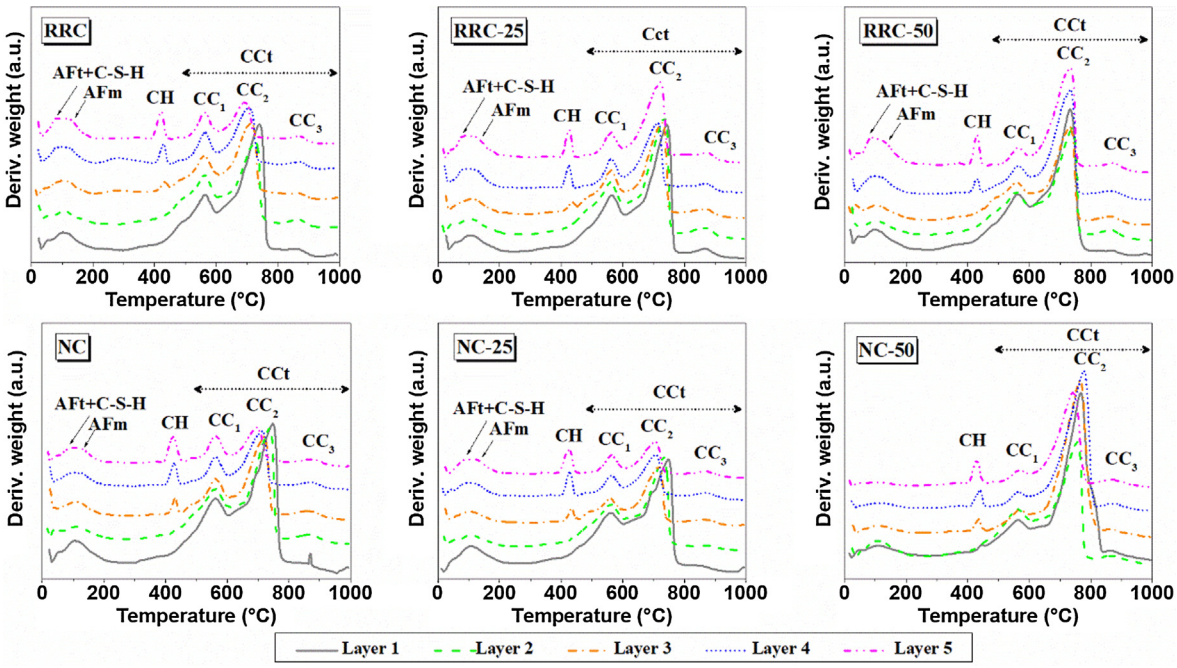

Fig. 11. DTG curves for five layers in 56 d samples (innermost to outermost layer shown from top down in each graph).

Earlier DTA/TG studies, in conjunction with mass spectroscopic analysis, have shown that the gas released in the 550 °C to 600 °C range is CO_2, associated with amorphous carbonate decomposition [13]. Some authors contend that such amorphous or poorly crystallised carbonates and the metastable $CaCO_3$ polymorphs are generally the result of C-S-H gel carbonation [14]. Further to those data, the signal at 560 °C to 564 °C (CC_1) was probably due to amorphous phase or metastable $CaCO_3$ decomposition, the peak at 700 °C to 748 °C (CC_2) to poorly crystallised calcite decomposition and the signal at 860 °C to 879 °C (CC_3) to perfectly crystallised calcite decomposition. Whilst the literature often attributes the peak at 700 °C to 748 °C to aragonite and vaterite decomposition [14], that possibility was not envisaged here in light of earlier studies showing that after sample calcination at 600 °C only calcite is identifiable in XRD analysis [85]. Regardless of the calcium carbonate polymorph generating each signal, signal CC_2 was observed to shift to higher temperatures as the depth from the surface declined (values of 700 °C for layer 5 compared to 750 °C for layer 1), whereas signal CC_1 widened and became more asymmetrical.

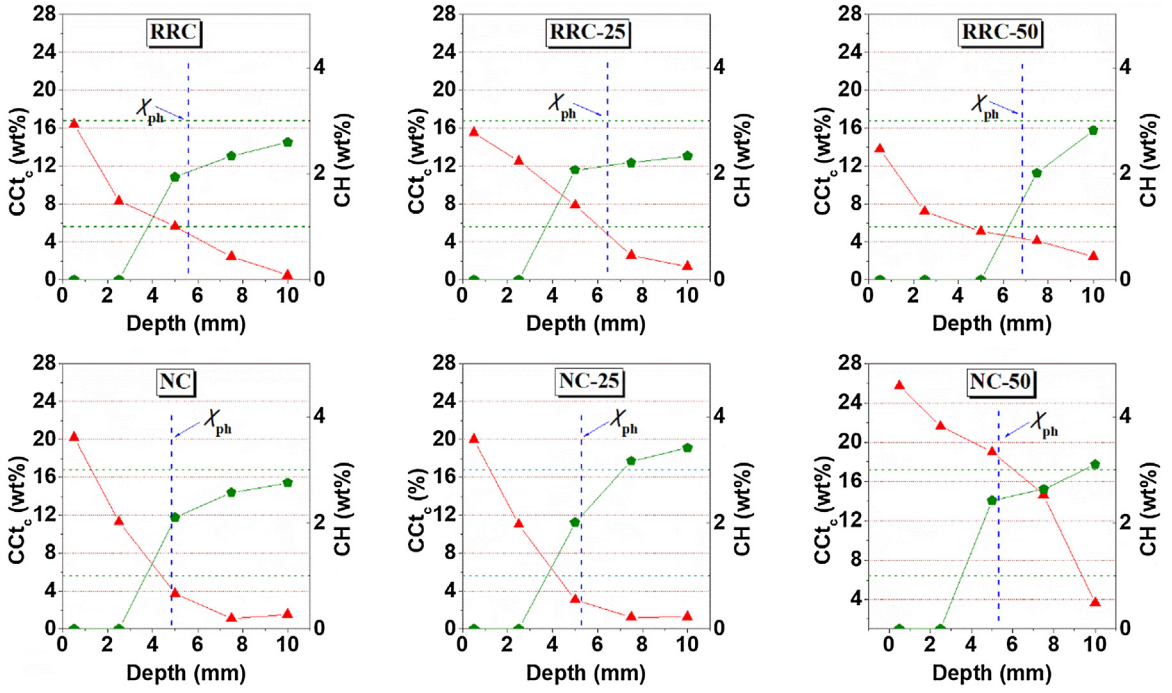

Fig. 12. Carbonation profile obtained by quantifying total $Ca(OH)_2$ and $CaCO_3$ from the TGA for 56 d samples (circle; CH; triangle: CCt; vertical dashed line: carbonation depth as determined by the phenolphthalein method).

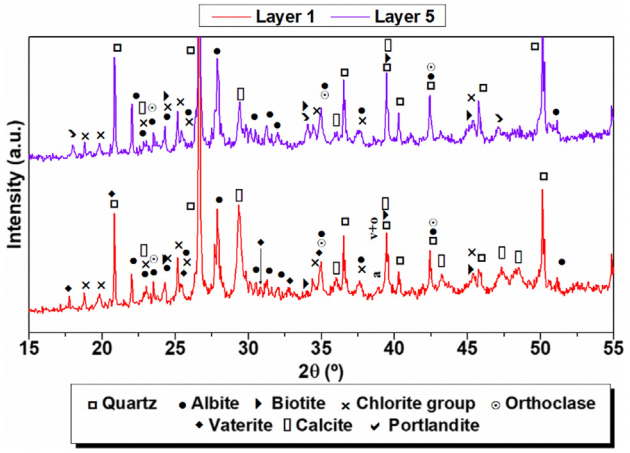

Fig. 13. XRD patterns for outermost layer 1 (below) and the innermost layer 5 (above) in the 56 d carbonated RRC-50 sample.

The DTG curves also showed that in all the samples the shallowest layer (closest to CO_2 exposure) exhibited more carbonates and no CH. Calcium hydroxide was first detected in layer 3 (6 mm) in all the samples except RRC-50, where it first appeared in layer 4 (7.5 mm). Those values were close to the mean carbonation depth (taking the standard deviation into consideration) found using the phenolphthalein method. Consequently, no CH was detected between the exposed surface and the mean carbonation depth identified by the aforementioned method.

Fig. 12 shows that more carbonates precipitated and CH disappeared at higher degrees of carbonation (layer closest to the CO_2-exposed surface) and that the carbonation depth identified with the phenolphthalein spray was close to the point where CH rose abruptly and CCt_c declined. Assuming the carbonation depth determined by TG to be the point where CH and CCt_c became nearly constant yielded values of 7.5 mm for NC, 8.0 mm for NC-25 and 10.0 mm for NC-50; and 8.0 mm for RRC, 8.5 mm for RRC-25 and 10.0 mm for RRC-50. Those values were higher than found with the phenolphthalein spray, a pattern also observed by other authors [76,86].

Another finding gleaned from Fig. 12 is that the amount of portlandite in the deepest layer, where the sample was uncarbonated, was slightly lower in the samples containing recycled cement (RRC, RRC-25 and RRC-50) than in the OPC-based concretes (NC, NC-25 and NC-50) due to the pozzolanic reaction induced by the addition.

The calcium carbonate polymorphs, which are difficult to identify with DTA and DTG, can in some cases be detected with X-ray diffraction. A number of authors [13,72,84,85,87] identified the formation of the three calcium carbonate polymorphs (vaterite, aragonite and calcite) in synthetic tobermorite, cement paste or synthetic C-S-H gel carbonation at relatively low or moderate (1% to 10%) CO_2 concentrations and moderate relative humidity (50% to 75%). Studies [13] analysing different CO_2 concentrations showed that scantly metastable aragonite formed and that vaterite formation was favoured at relatively low CO_2 concentrations. Here only calcite could be unequivocally identified. Vaterite may have been present in the outermost layer (layer 1), whereas in the innermost layer (layer 5) only calcite was detected and the intensity of its reflection was lower, as shown by way of example in the diffractogram for RRC-50 (Fig. 13). No CH was found on the diffractogram for layer 1, whereas it was identifiable at layer 5, corroborating the differential thermal analysis data.

The FTIR study conducted on sample RRC-50 (Fig. 14) confirmed the DTG data, i.e., the absence of CH in the outermost and its presence in the innermost layer (bands at 3642 cm^{-1} and 3530 cm^{-1}. The carbonate bands present in both the calcite and vaterite polymorphs at 875 cm^{-1} (ν_2 O-C-O out-of-plane bending vibrations

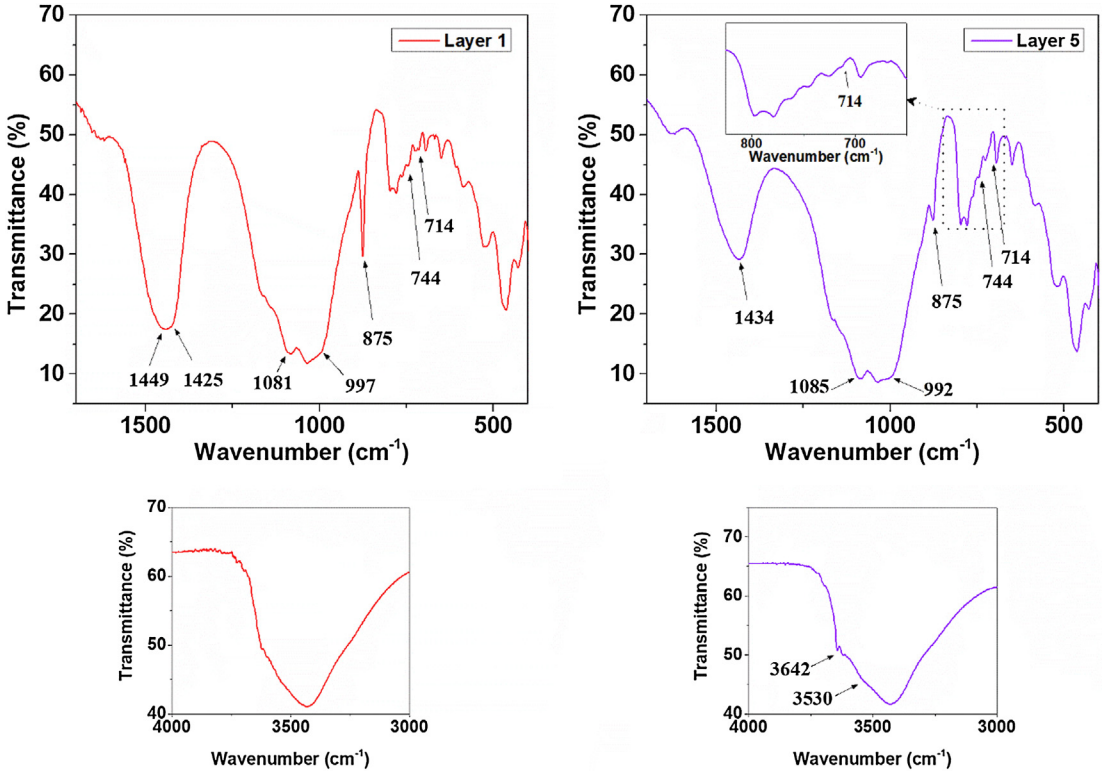

Fig. 14. FTIR spectra for the layers closest to and farthest from the CO_2 exposure surface in the 56 d carbonated RRC-50 sample.

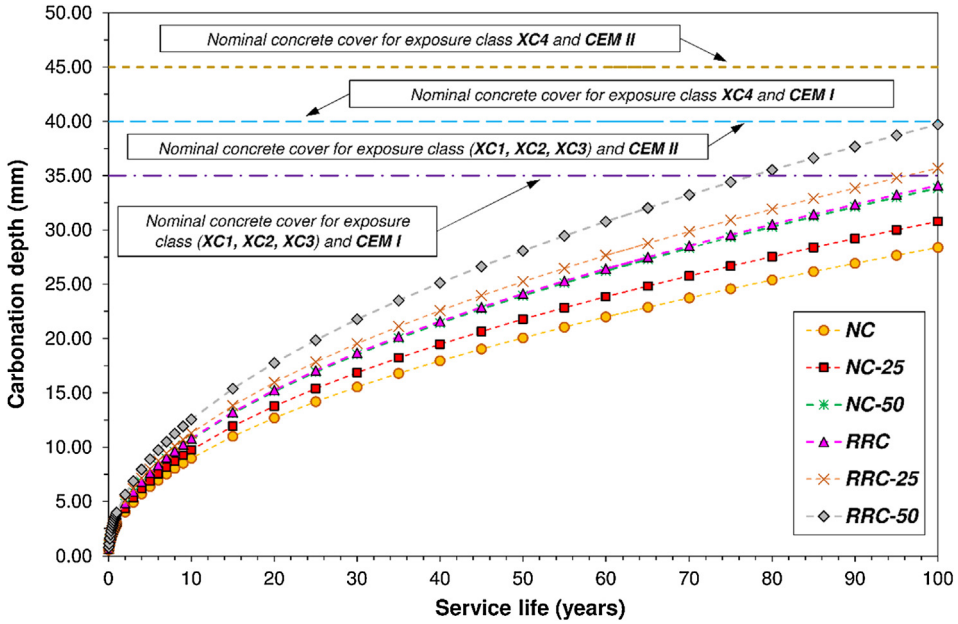

Fig. 15. Service life as predicted by the model proposed in EHE-08.

[88]); and a very intense band at 1400 cm^{-1} to 1500 cm^{-1} (ν_3 C-O asymmetric stretching vibrations) were more intense in the layer 1 spectrum. Nonetheless, as in XRD, vaterite formation was not clearly identified at this depth because its characteristic bands overlapped greatly with those of other phases. The band at 1085 cm^{-1}, for instance, overlapped with the chlorite and quartz group band and the one at 744 cm^{-1} with the albite band. In contrast, calcite could be identified on the FTIR spectrum thanks to the presence of one of its characteristic signals at 714 cm^{-1} (ν_4 O-C-O in-plane bending vibrations [88]).

The bands for C-S-H gel in hydrated cements appear at around 970 cm^{-1} to 980 cm^{-1} (stretching vibrations generated by Q^2 Si-O tetrahedra) and at 450 cm^{-1} to 500 cm^{-1} (O-Si-O bending vibrations) [89]. The FTIR spectrum for layer 5, the uncarbonated part of the sample, exhibited a band attributable to Q^2 unit Si-O stretching vibrations at around 992 cm^{-1}, a value slightly higher than normally associated with this band, very likely due to overlapping with bands for other phases (chlorite group). On the layer 1 spectrum, the same band was shifted to an even higher wavenumber, 997 cm^{-1}. That shift in Q^2 unit stretching vibrations is associated with a longer mean chain length (MCL) in the C-S-H gel. According to the literature [90], the calcium ions in the C-S-H gel interlayer are eliminated during carbonation, generating a charge imbalance, which is compensated primarily by protonation and the subsequent formation of Si-OH groups. Neighbouring Si-OH groups consequently condense as in the following reaction: ≡Si—OH + OH—Si≡ → ≡Si—O—Si≡ + H_2O. The outcome is a longer mean chain length in the C-S-H gel and a decline in its Ca/Si ratio. No perceptible changes due to CO_2 exposure were observed in the O-Si-O bending vibration region.

3.6. Service life prediction

Fig. 15 shows the carbonation depth throughout the service life of a concrete member exposed to class XC1, XC2, XC3 or XC4 environments, i.e. at risk of carbonation-induced corrosion, estimated by the model proposed in Spain's structural concrete code EHE-08 (Eq. (9)), which assumes constant CO_2 diffusion across the entire service life [3].

Table 7
Minimum cover required and estimated depassivation time in the concretes analysed further to the prediction model used.

Concrete mix	Minimum cover (mm)	Depassivation time (years)	
		XC1, XC2, XC3	XC4
NC	29	167	218
NC-25	31	142	185
NC-50	34	117	153
RRC	35	151	191
RRC-25	36	138	174
RRC-50	40	111	141

Based on the cover recommended by EHE-08 by type of cement and exposure class (also shown in the figure), after 100 years of service, the CO_2 penetration front would not have reached the reinforcement in any of the concretes designed.

Table 7 depicts the minimum design cover ($c_{min,dur}$) required for a 100 year service life for the concretes analysed under the environmental conditions stipulated in the prediction model used. The $C_{min,dur}$ values stipulated in Eurocode EN 1992-1-1 [91] are 20 mm for exposure class XC1, 30 mm for XC2 and XC3 and 40 mm for XC4. Further to EHE-08 model results, designers could reduce the minimum cover recommended for exposure classes XC2 and XC3 in concretes NC and NC-25 and for exposure class XC4 in all the concretes analysed. Reducing the concrete cover without jeopardising the safe transfer of bonding stress or reducing fire resistance entails economic, environmental and design benefits and favours shape optimisation of structural members.

In the concretes studied, steel depassivation would take over 111 years in exposure classes XC1, XC2 and XC3 and over 141 years in class XC4 (Table 7). These findings show that carbonation-associated corrosion would not pose a safety problem at any time during the structure's service life. Furthermore, as concretes exposed to XC4 environments are not in constant contact with water, the concomitant irregular wet/dry cycles might retard CO_2 diffusion and lengthen the time needed for the depassivation of reinforcement embedded in concrete [45].

4. Conclusions

The conclusions that can be drawn from the present study are listed below.

- Replacing 25 wt% of natural aggregate with mixed recycled aggregate induces no statistically significant effect on CO_2 penetration, whereas that parameter is significantly impacted ($p < 0.05$) when a 50% replacement ratio is used.
- The mean carbonation depth in concretes with 25% recycled aggregate is 1.07 times greater and in materials with 50% replacement 1.18 times greater than in conventional concretes with natural aggregate.
- The use of cement with 25% fired clay-based construction and demolition waste induces a significant increase in CO_2 penetration, irrespective of exposure time and percentage of mixed recycled aggregate: the mean carbonation depth in concretes with cement containing recycled material is approximately 1.20 times greater than in concrete with conventional cement.
- Regardless of cement type and percentage of recycled aggregate, the CO_2 penetration coefficient is below the 4 mm/year$^{0.5}$ indicative of good quality concrete.
- Splitting tensile strength rises with time of exposure to carbonation in the concretes tested.
- Carbonation prompts a decline in open porosity, more intensely in concretes with a higher carbonation rate.
- The inclusion of mixed recycled aggregate and cement containing CW does not compromise reinforcement passivity, according to EHE-08 service life prediction models.
- The minimum design cover recommended in Eurocode EN 1992-1-1 for exposure class XC4 could be reduced in members manufactured with the new concretes studied.
- In light of the present findings and in terms of concrete permeability to gas, natural aggregate can be viably replaced with mixed recycled aggregate separately or in conjunction with the use of fired clay-based C&DW cement.
- The carbonation depth found with the phenolphthalein method is shallower than observed with TG, defining carbonation depth in the latter as the point where CH and CCt_c stabilise to constant levels.
- DTG curves show that no calcium hydroxide is detected between the exposed surface and the mean carbonation depth identified by the phenolphthalein method. The first layer where CH is detected by DTA/DTG concurs with the mean carbonation depth found with the phenolphthalein method.
- According to XRD analysis, of the calcium carbonate polymorphs, only calcite (indisputably) and vaterite (possibly) are present in the layer closest to CO_2 exposure, whereas only calcite is found in the layer farthest from the exposure surface.
- The FTIR findings show that the band attributable to Q^2 unit Si-O stretching vibrations shifts to a higher wavenumber in the layer closest to CO_2 exposure.

Declaration of Competing Interest

The authors declare that they have no known competing financial interests or personal relationships that could have appeared to influence the work reported in this paper.

Acknowledgements

This study was funded under research projects BIA 2013-48876-C3-1-R, BIA2013-48876-C3-2-R and BIA2016-76643-C3-1-R awarded by the Ministry of Science and Innovation and grant GR 18122 awarded to the MATERIA Research Group by the Regional Government of Extremadura and the European Regional Development Fund, ERDF. In 2016 University of Extremadura teaching and research personnel benefitted from a mobility grant (MOV15A029) awarded by the Regional Government of Extremadura and in 2018 from a José Castillejo (CAS17/00313) scholarship granted by the Spanish Ministry of Education, Culture and Sport.

Philip Van den Heede is since October 2017 a postdoctoral fellow of the Research Foundation—Flanders (FWO) (project number 3E013917) and acknowledges its support.

The experimental procedures for this study were largely conducted at the Magnel Laboratory for Concrete Research, Belgium, in conjunction with the University of Extremadura and Spain's Scientific Research Council on the occasion of the first and last (and senior) authors' participation in a visiting scholar programme.

The assistance of Messrs Blas Cantero Chaparro and Pablo Plaza Caballero in concrete manufacture is gratefully acknowledged.

Appendix A. Supplementary data

Supplementary data to this article can be found online at https://doi.org/10.1016/j.conbuildmat.2019.117336.

References

[1] European Committee for Standardization, EN 206-1:2008. Concrete. Part 1: Specification, performance, production and conformity.
[2] European Committee for Standardization, EN 1992-1-1. Eurocode 2: Design of concrete structures. Parte 1-1: General rules and rules for building.
[3] Comisión Permanente del Hormigón, Instrucción Hormigón Estructural. EHE-08, First Edition, Ministerio de Fomento. Centro de Publicaciones, Madrid, 2008.
[4] International Federation for Structural Concrete, fib Model Code for Concrete Structures 2010, Lausanne, Switzerland, 2013.
[5] A. Köliö, T.A. Pakkala, J. Lahdensivu, M. Kiviste, Durability demands related to carbonation induced corrosion for Finnish concrete buildings in changing climate, Eng. Struct. 62–63 (2014) 42–52.
[6] N. Singh, M. Mithulraj, S. Arya, Influence of coal bottom ash as fine aggregates replacement on various properties of concretes: a review, Resour. Conserv. Recycl. 138 (2018) 257–271.
[7] P.F. Marques, C. Chastre, Â. Nunes, Carbonation service life modelling of RC structures for concrete with Portland and blended cements, Cem. Concr. Compos. 37 (2013) 171–184.
[8] L.J. Parrott, Some effects of cement and curing upon carbonation and reinforcement corrosion in concrete, Mater. Struct. 29 (1996) 164.
[9] W. Renpu, Chapter 11 - oil and gas well corrosion and corrosion prevention, in: W. Renpu (Ed.), Advanced Well Completion Engineering, third ed., Gulf Professional Publishing, 2011, pp. 617–700.
[10] E. Possan, W.A. Thomaz, G.A. Aleandri, E.F. Felix, A.C.P. dos Santos, CO2 uptake potential due to concrete carbonation: a case study, Case Stud. Constr. Mater. 6 (2017) 147–161.
[11] N. Singh, S.P. Singh, Reviewing the carbonation resistance of concrete, J. Mater. Eng. Struct. 3 (2016) 35–57.
[12] F. Glasser, T. Matchei, Interactions between portland cement and carbon dioxide Montreal, Canada, XII International Congress of Cement Chemistry (ICC), 2007.
[13] A. Morandeau, M. Thiéry, P. Dangla, Investigation of the carbonation mechanism of CH and C-S-H in terms of kinetics, microstructure changes and moisture properties, Cem. Concr. Res. 56 (2014) 153–170.
[14] M. Thiery, G. Villain, P. Dangla, G. Platret, Investigation of the carbonation front shape on cementitious materials: effects of the chemical kinetics, Cem. Concr. Res. 7 (2007) 1047–1058.
[15] A. Köliö, P.J. Niemelä, J. Lahdensivu, Evaluation of a carbonation model for existing concrete facades and balconies by consecutive field measurements, Cem. Concr. Compos. 65 (2016) 29–40.
[16] F. Pacheco Torgal, S. Miraldo, J.A. Labrincha, J. De Brito, An overview on concrete carbonation in the context of eco-efficient construction: evaluation, use of SCMs and/or RAC, Constr. Build. Mater. 36 (2012) 141–150.
[17] S.O. Ekolu, Model for practical prediction of natural carbonation in reinforced concrete: part 1-formulation, Cem. Concr. Compos. 86 (2018) 40–56.
[18] K. Zhang, J. Xiao, Prediction model of carbonation depth for recycled aggregate concrete, Cem. Concr. Compos. 88 (2018) 86–99.
[19] C. Meyer, The greening of the concrete industry, Cem. Concr. Compos. 31 (2009) 601–605.
[20] H. Guo, C. Shi, X. Guan, J. Zhu, Y. Ding, T.-C. Ling, H. Zhang, Y. Wang, Durability of recycled aggregate concrete – a review, Cem. Concr. Compos. 89 (2018) 251–259.

[21] M. Gomes, J. de Brito, Structural concrete with incorporation of coarse recycled concrete and ceramic aggregates: durability performance, Mater. Struct. 42 (2009) 663–675.
[22] P.S. Lovato, E. Possan, D.C.C.D. Molin, Â.B. Masuero, J.L.D. Ribeiro, Modeling of mechanical properties and durability of recycled aggregate concretes, Constr. Build. Mater. 26 (2012) 437–447.
[23] C.J. Zega, Á.A. Di Maio, Use of recycled fine aggregate in concretes with durable requirements, Waste Manage. 31 (2011) 2336–2340.
[24] L. Evangelista, J. de Brito, Durability performance of concrete made with fine recycled concrete aggregates, Cem. Concr. Compos. 32 (2010) 9–14.
[25] F. Faleschini, M.A. Zanini, L. Hofer, Reliability-based analysis of recycled aggregate concrete under carbonation, Adv. Civ. Eng. (2018) 4742372.
[26] C. Medina, M.I. Sánchez de Rojas, C. Thomas, J.A. Polanco, M. Frías, Durability of recycled concrete made with recycled ceramic sanitary ware aggregate. Inter-indicator relationships, Constr. Build. Mater. 105 (2016) 480–486.
[27] C. Medina, M. Frías, M.I. Sánchez de Rojas, C. Thomas, J.A. Polanco, Gas permeability in concrete containing recycled ceramic sanitary ware aggregate, Constr. Build. Mater. 37 (2012) 597–605.
[28] S.M. Levy, P. Helene, Durability of recycled aggregates concrete: a safe way to sustainable development, Cem. Concr. Res. 34 (2004) 1975–1980.
[29] T. Vieira, A. Alves, J. de Brito, J.R. Correia, R.V. Silva, Durability-related performance of concrete containing fine recycled aggregates from crushed bricks and sanitary ware, Mater. Des. 90 (2016) 767–776.
[30] M. Bravo, J. de Brito, L. Evangelista, J. Pacheco, Durability and shrinkage of concrete with CDW as recycled aggregates: benefits from superplasticizer's incorporation and influence of CDW composition, Constr. Build. Mater. 168 (2018) 818–830.
[31] V.W.Y. Tam, M. Soomro, A.C.J. Evangelista, A review of recycled aggregate in concrete applications (2000–2017), Constr. Build. Mater. 172 (2018) 272–292.
[32] C. Medina, W. Zhu, T. Howind, M.I. Sanchez de Rojas, M. Frias, Influence of mixed recycled aggregate on the physical – mechanical properties of recycled concrete, J. Clean Prod. 68 (2014) 216–225.
[33] M.I. Sánchez de Rojas, M. Frías, E. Asensio, C. Medina, Residuo cerámico útil para la elaboración de cementos, procedimiento de obtención y cementos que lo comprende (ES2512065), Consejo Superior de Investigaciones Científicas (CSIC), 2016. Spain.
[34] European Committee for Standardization, EN 1097-6:2014. Tests for mechanical and physical properties of aggregates - Part 6: Determination of particle density and water absorption.
[35] European Committee for Standardization, EN 933-3. Tests for geometrical properties of aggregates - Part 3: Determination of particle shape - Flakiness index.
[36] European Committee for Standardization, EN 1097-2. Tests for mechanical and physical properties of aggregates - Part 2: Methods for the determination of resistance to fragmentation.
[37] European Committee for Standardization, EN 197-1. Cement - Part 1: Composition, specifications and conformity criteria for common cements.
[38] American Society for Testing and Materials, ASTM C618-15. Standard specification for coal fly ash and raw or calcined natrual pozzolan for use in concrete
[39] E. Asensio, C. Medina, M. Frías, M.I. Sánchez de Rojas, Design of eco-efficient cements bearing construction and demolitions waste as a pozzolan addition, J. Clean Prod. [Under review].
[40] D.C. Teychenné, R.E. Franklin, H.C. Erntroy, Design of Normal Concrete Mixes, second ed., IHS BRE Press, Garston, Watford, 2010.
[41] B. Cantero, I.F. Sáez del Bosque, A. Matías, C. Medina, Statistically significant effects of mixed recycled aggregate on the physical-mechanical properties of structural concretes, Constr. Build. Mater. 185 (2018) 93–101.
[42] Bureau for Standardisation, NBN B 05-201. Resistance of materials to freezing - Water absorption by capillarity, in, Belgium, 1976.
[43] Spanish Committee for Standardization, UNE 83993-2. Durability of concrete. Test method. Measurement of carbonation penetration rate in hardened concrete. Part 2: Accelerated method.
[44] Spanish Committee for Standardization, UNE 112011. Corrosion of concrete reinforcement steel. Determination of the carbonatation depht for in-service concrete.
[45] P. Van den Heede, N. De Belie, A service life based global warming potential for high-volume fly ash concrete exposed to carbonation, Constr. Build. Mater. 55 (2014) 183–193.
[46] E.I. Moreno, Carbonation coefficients from concrete made with high-absorption limestone aggregate, Adv. Mater. Sci. Eng. (2013).
[47] I.F. Sáez del Bosque, W. Zhu, T. Howind, A. Matías, M.I. Sánchez de Rojas, C. Medina, Properties of interfacial transition zones (ITZs) in concrete containing recycled mixed aggregate, Cem. Concr. Compos. 81 (2017) 25–34.
[48] C. Medina, W. Zhu, T. Howind, M.I.S. De Rojas, M. Frías, Influence of interfacial transition zone on engineering properties of the concrete manufactured with recycled ceramic aggregate, J. Civ. Eng. Manage. 21 (2015) 83–93.
[49] A. Leemann, P. Nygaard, J. Kaufmann, R. Loser, Relation between carbonation resistance, mix design and exposure of mortar and concrete, Cem. Concr. Compos. 62 (2015) 33–43.
[50] B. Šavija, M. Luković, Carbonation of cement paste: understanding, challenges, and opportunities, Constr. Build. Mater. 117 (2016) 285–301.
[51] N. Singh, S.P. Singh, Carbonation and electrical resistance of self compacting concrete made with recycled concrete aggregates and metakaolin, Constr. Build. Mater. 121 (2016) 400–409.
[52] M. Limbachiya, M.S. Meddah, Y. Ouchagour, Performance of Portland/silica fume cement concrete produced with recycled concrete aggregate, ACI Mater. J. 109 (2012) 91–100.
[53] S.-C. Kou, C.-S. Poon, Long-term mechanical and durability properties of recycled aggregate concrete prepared with the incorporation of fly ash, Cem. Concr. Compos. 37 (2013) 12–19.
[54] A.B. Ribeiro, T. Santos, A. Gonçalves, Performance of concrete exposed to natural carbonation: use of the k-value concept, Constr. Build. Mater. 175 (2018) 360–370.
[55] J. de Brito, J. Ferreira, J. Pacheco, D. Soares, M. Guerreiro, Structural, material, mechanical and durability properties and behaviour of recycled aggregates concrete, J. Build. Eng. 6 (2016) 1–16.
[56] C. Alexandridou, G.N. Angelopoulos, F.A. Coutelieris, Mechanical and durability performance of concrete produced with recycled aggregates from Greek construction and demolition waste plants, J. Clean. Prod. 176 (2018) 745–757.
[57] P. Amorim, J. de Brito, L. Evangelista, Concrete made with coarse concrete aggregate: influence of curing on durability, ACI Mater. J. 109 (2012) 195–204.
[58] N. Otsuki, S. Miyazato, W. Yodsudjai, Influence of recycled aggregate on interfacial transition zone, strength, chloride penetration and carbonation of concrete, J. Mater. Civ. Eng. 15 (2003) 443–451.
[59] BCSJ, Proposed standard for the use of recycled aggregate and recycled aggregate concrete (in Japanese), in, Committee on Disposal and Reuse of Construction, Japan, 1977.
[60] C. Faella, C. Lima, E. Martinelli, M. Pepe, R. Realfonzo, Mechanical and durability performance of sustainable structural concretes: an experimental study, Cem. Concr. Compos. 71 (2016) 85–96.
[61] J. Xiao, B. Lei, C. Zhang, On carbonation behavior of recycled aggregate concrete, Sci. China Technol. Sci. 55 (2012) 2609–2616.
[62] H. Gurdián, E. García-Alcocel, F. Baeza-Brotons, P. Garcés, E. Zornoza, Corrosion behavior of steel reinforcement in concrete with recycled aggregates, fly ash and spent cracking catalyst, Materials (Basel, Switzerland) 7 (2014) 3176–3197.
[63] F. Buyle-Bodin, R. Hadjieva-Zaharieva, Influence of industrially produced recycled aggregates on flow properties of concrete, Mater. Struct. 35 (2002) 504–509.
[64] D. Pedro, J. de Brito, L. Evangelista, Structural concrete with simultaneous incorporation of fine and coarse recycled concrete aggregates: mechanical, durability and long-term properties, Constr. Build. Mater. 154 (2017) 294–309.
[65] R.V. Silva, R. Neves, J. de Brito, R.K. Dhir, Carbonation behaviour of recycled aggregate concrete, Cem. Concr. Compos. 62 (2015) 22–32.
[66] N. Singh, S.P. Singh, Validation of carbonation behavior of self compacting concrete made with recycled aggregates using microstructural and crystallization investigations, Eur. J. Environ. Civ. Eng. (2018) 1–24.
[67] European Comitte for Standardisation, prCEN/TS 12390-12. Testing of hardened concrete. Part 12: Determination of the carbonation resistance of concrete. Accelerated carbonation method.
[68] A.M. Neville, Properties of Concrete, first ed., Longman Scientific & Technical John Wiley & Sons, Harlow (New York), 2008.
[69] O. Trocónis-Rincón, A. Romero-Carruyo, C. Andrade, P. Helene, I. Díaz, Manual for Inspecting, Evaluating and Diagnosing Corrosion in Reinforced Concrete Structures, Maracaibo, Venezuela, 2000.
[70] M.A. Sanjuán, C. del Olmo, Carbonation resistance of one industrial mortar used as a concrete coating, Build. Environ. 36 (2001) 949–953.
[71] S. Greve-Dierfeld, C. Gehlen, Performance-based durability design, carbonation part 2 – classification of concrete, Struct. Concr. 17 (2016) 523–532.
[72] V. Shah, K. Scrivener, B. Bhattacharjee, S. Bishnoi, Changes in microstructure characteristics of cement paste on carbonation, Cem. Concr. Res. 109 (2018) 184–197.
[73] P.C. Hewlett, Leás Chemistry of Cement and Concrete, fourth ed., 1998. London.
[74] P.H.R. Borges, J.O. Costa, N.B. Milestone, C.J. Lynsdale, R.E. Streatfield, Carbonation of CH and C-S–H in composite cement pastes containing high amounts of BFS, Cem. Concr. Res. 40 (2010) 284–292.
[75] Q. Shen, G. Pan, B. Bao, Influence of CSH carbonation on the porosity of cement paste, Mag. Concr. Res. 68 (2016) 504–514.
[76] B. Wu, G. Ye, Development of porosity of cement paste blended with supplementary cementitious materials after carbonation, Constr. Build. Mater. 145 (2017) 52–61.
[77] E. Gruyaert, P. Van den Heede, N. De Belie, Carbonation of slag concrete: effect of the cement replacement level and curing on the carbonation coefficient – effect of carbonation on the pore structure, Cem. Concr. Compos. 35 (2013) 39–48.
[78] W. Ashraf, J. Olek, Elucidating the accelerated carbonation products of calcium silicates using multi-technique approach, J. CO2 Util. 23 (2018) 61–74.
[79] S.-W. Lee, Y.-J. Kim, Y.-H. Lee, H. Guim, S.M. Han, Behavior and characteristics of amorphous calcium carbonate and calcite using $CaCO_3$ film synthesis, Mater. Des. 112 (2016) 367–373.
[80] J. Perić, M. Vučak, R. Krstulović, L. Brečević, D. Kralj, Phase transformation of calcium carbonate polymorphs, Thermochim. Acta 277 (1996) 175–186.
[81] E.T. Stepkowska, M.A. Aviles, J.M. Blanes, J.L. Perez-Rodriguez, Gradualtransformation of $Ca(OH)_2$ into $CaCO_3$on cement hydration, J. Therm. Anal. Calorim. 87 (2007) 189–198.
[82] J. Perić, R. Krstulović, T. Ferić, M. Vučak, The examination of the phase transformation of aragonite into calcite by means of DSC analysis, Thermochim. Acta 207 (1992) 245–254.

[83] V.S. Ramachandran, R.M. Paroli, J.J. Beaudoin, A.H. Delgado, Handbook of Thermal Analysis of Construction Materials, William Andrew Publishing, Norwich, NY, 2002.
[84] Z. Šauman, Carbonization of porous concrete and its main binding components, Cem. Concr. Res. 1 (1971) 645–662.
[85] J. Chang, Y. Fang, Quantitative analysis of accelerated carbonation products of the synthetic calcium silicate hydrate(C–S–H) by QXRD and TG/MS, J. Therm. Anal. Calorim. 119 (2015) 57–62.
[86] C.-F. Chang, J.-W. Chen, The experimental investigation of concrete carbonation depth, Cem. Concr. Res. 36 (2006) 1760–1767.
[87] M. Auroy, S. Poyet, P. Le Bescop, J.-M. Torrenti, T. Charpentier, M. Moskura, X. Bourbon, Comparison between natural and accelerated carbonation (3% CO2): impact on mineralogy, microstructure, water retention and cracking, Cem. Concr. Res. 109 (2018) 64–80.
[88] Ö. Cizer, C. Rodriguez-Navarro, E. Ruiz-Agudo, J. Elsen, D. Van Gemert, K. Van Balen, Phase and morphology evolution of calcium carbonate precipitated by carbonation of hydrated lime, J. Mater. Sci. 47 (2012) 6151–6165.
[89] P. Yu, R.J. Kirkpatrick, B. Poe, P.F. McMillan, X. Cong, Structure of calcium silicate hydrate (C-S-H): near-, mid-, and Far-Infrared Spectroscopy, J. Am. Ceram. Soc. 82 (1999) 742–748.
[90] J.J. Chen, J.J. Thomas, H.M. Jennings, Decalcification shrinkage of cement paste, Cem. Concr. Res. 36 (2006) 801–809.
[91] European Committee for Standardization, EN 1992-1-1. Eurocode 2: Design of concrete structures. Parte 1-1: General rules and rules for building.